Deep Learning in Forest Structural Parameter Estimation Using Airborne LiDAR Data

Hao Liu, Xin Shen, Lin Cao, Ting Yun, Zhengnan Zhang, Xiaoyao Fu, Xinxin Chen, and Fangzhou Liu

***Abstract*—Accurately estimating and mapping forest structural parameters are essential for monitoring forest resources and understanding ecological processes. The novel deep learning algorithm has the potential to be a promising approach to improve the estimation accuracy while combining with advanced remote sensing technology. Airborne light detection and ranging (LiDAR) has the preferable capability to characterize 3-D canopy structure and estimate forest structural parameters. In this study, we developed a deep learning-based algorithm (Deep-RBN) that combined the fully connected network (FCN) deep learning algorithm with the optimized radial basis neural network (RBN) algorithm for forest structural parameter estimation using airborne LiDAR data. The multiple iterations were used to constantly update the internal weights to achieve the optimized accuracy of model fitting, and the optimized RBN algorithm was developed for the limited training sets. We assessed the efficiency and capability of the Deep-RBN in the estimation of forest structural parameters in a subtropical planted forest of southern China, by comparing the traditional FCN algorithm and multiple linear regression. We found that Deep-RBN had the strongest capability in estimates of forest structural parameters (R^2 = 0.67–0.86, rRMSE = 6.95%–20.34%). The sensitivity analysis of the key hyperparameters of Deep-RBN algorithm showed that the learning rate is one of the most important parameters that influence the performance of predictive models, and while its value equal is to 0.001, the predictive models had the highest accuracy (mean DBH: RMSE = 1.01, mean height: RMSE = 1.45, volume: RMSE = 26.49, stem density: RMSE = 121.06). With the increase of training samples added in Deep-RBN model, the predictive models performed better; however, no significant improvements of accuracy were observed while the number of training set is larger than 80. This study demonstrates the benefits of jointly using the Deep-RBN algorithm and airborne LiDAR data to improve the accuracy of forest structural parameter estimation and mapping, which provides a promising methodology for sustainable forest resources monitoring.**

***Index Terms*—Deep learning, forest structural parameters, hyperparameter, LiDAR, volume distribution.**

Manuscript received October 24, 2020; accepted December 15, 2020. Date of publication December 21, 2020; date of current version January 11, 2021. This work was supported by in part by the National Key R&D Program of China under Grant 2017YFD0600904, in part by the National Natural Science Foundation of China under Grant 31770590, and in part by the Priority Academic Program Development of Jiangsu Higher Education Institutions (PAPD). *(Hao Liu and Xin Shen are co-first authors.) (Corresponding author: Lin Cao.)*

Hao Liu, Xin Shen, Lin Cao, Zhengnan Zhang, and Xiaoyao Fu are with the Co-Innovation Center for Sustainable Forestry in Southern China, Nanjing Forestry University, Nanjing 210037, China (e-mail: liuhao_njfu@hotmail.com; shenxin1903@gmail.com; lincao@njfu.edu.cn; zhangzhengnan_njfu@hotmail.com; fuxyrainlan@gmail.com).

Ting Yun, Xinxin Chen, and Fangzhou Liu are with the College of Information Science and Technology, Nanjing Forestry University, Nanjing 210037 China (e-mail: njyunting@gmail.com; 15950569238@163.com; liufangzhou@njfu.edu.cn).

Digital Object Identifier 10.1109/JSTARS.2020.3046053

I. Introduction

As THE important component of terrestrial ecosystems, forest plays a crucial role in global climate change mitigation [1], ecological services supplement [2], and biodiversity protection [3]. In recent years, due to intensive timber harvesting and silviculture activities, forests changed and updated rapidly [4], [5], resulting in lots of new challenges for forest sustainable management and forest inventory. The demands of increased information are urgent for assessing the composition and structure of forest biomes [6]. Thus, accurate, effective, and timely characterization of forest structural parameters is essential for forest sustainable management [7].

In the past decades, forest resource management benefited from the increased available remote sensing (RS) data and enhanced forest inventories [8] that had proven helpful to optimize management planning [9], [10], understand forest carbon cycling [11], and support forest inventory [12]. Airborne light detection and ranging (LiDAR) is an active RS technology, which has the capability to measure 3-D forest canopy structure [13]–[15] and characterize vertical profiles [16]. In EFI practice, it has been proved that airborne LiDAR has the advantages of robustness and portability in estimating forest structural parameters with area-based approach (ABA) [17]–[19].

The statistical relationships between airborne LiDAR-derived point cloud metrics and filed measurements of forest stands were commonly used for wall-to-wall forest structural parameter prediction or mapping [17]. Usually, the modeling approaches can be categorized as parametric [20]–[22] and nonparametric [23]–[25] regression methods. Parametric methods, such as multiple linear regression (MLR) relied on numerous assumptions (e.g., normality, homoscedasticity, and linearity) [26] and had the issue of multicollinearity [27], [28]. Nevertheless, nonparametric methods, such as machine learning-based algorithms [e.g., random forest (RF), artificial neural networks (ANN)], made no strict assumptions and generally employed faster, and were more accurate than parametric methods [29]. They have been increasingly applied with popularity in the RS community [30], [31]. In recent years, ANN was designed to simulate the way of brain neural network processing and memory information [32]. Özçelik *et al.* (2013) used back-propagation ANN models and other regression algorithms to estimate individual-tree height in Turkey. It was indicated that ANN was a reliable algorithm that had the best generalization ability [33]. Nunes and Görgens (2016) compared classical machine learning algorithms for forest structural parameter estimation for complex vegetation mosaic in Brazil; they found that the ANN performed better

than RF. They suggested artificial intelligence tools (i.e., neural networks) be used in forestry applications [34].

Deep learning has become the most popular algorithm of artificial intelligence [35]–[37]. It conducts complex tasks by automatically learning representations from raw input data and across multilayer neural networks that the backpropagation algorithm is applied to automatically optimize internal parameters [37], [38]. Comparing with traditional machine learning, deep learning is a completely data-driven algorithm to generate the best ways for feature extractions [39]. It exclusively learned complex hierarchical structures from RS dataset [40], rather than relying on a predesigned, specific algorithm [37]. Besides, it learned preknowledge from training data that contain noise, thus, has certain fault tolerance and generalization [41].

Deep learning algorithms are taking off in various remote sensing applications, such as image classification [42], high resolution imagery interpretation [43], multimodal data fusion [44], and target recognition [45]. Different RS data were used in deep learning studies, such as satellite images [46], hyperspectral images [47], SAR images [48], and LiDAR [49]. Image-based deep learning studies focused on extracting spectral and spatial features of RS images [50]. Convolution neural network (CNN) framework was one of the most successful deep learning frameworks for image feature representations by a combination of convolutional and pooling layers [40], [50]. For instance, previous studies applied CNNs for hyperspectral image classification, such as 1D-CNN in spectral domain [51], 2D-CNN in spatial domain [52], and 3D-CNN in both spectral and spatial domain [53]. Recurrent neural network (RNN) framework has popularly applied RS images with sequential data analysis in temporal domain [47], [50], [54].

Different from image-based studies, point cloud-based deep learning studies benefited from LiDAR or structure-from-motion (SFM) techniques that characterized 3-D structure information of objects [49]. Guan *et al.* (2015) earlier used mobile LiDAR data to examine deep learning methods for tree species classification, resulting in improved classification accuracy (overall accuracy: 86.1%). Wang *et al.* (2019) examined Faster R-CNN algorithms of deep learning for individual tree segmentation based on ground-based LiDAR data. They converted point clouds to deep images as input using a voxelization method for further analysis. Recently, raw point-based algorithms that directly consumed raw point cloud without transformation were proposed, including PointNet [57] and PointNet++ [58]. They considered the invariance of point cloud arrangement for applications of 3-D object detection, classification, and segmentation [49]. It has shown a promising prospect in combination with deep learning algorithms and point clouds.

In enhanced forest inventory studies, LiDAR-derived metrics are related to vegetation height or density and represented the vertical distribution of vegetation within the forest canopy [17]. Unlike raw point clouds required by point-based algorithms (e.g., PointNet, PointNet++), LiDAR metrics characterized structural features of point clouds, which could be more conveniently learned by deep learning algorithms. Then, the statistical relationships between LiDAR-derived metrics and ground plot measurements were generated for forest structural parameter modeling, which was significant in forest resource management. However, very few studies focus on deep learning regression algorithms for predicting forest structural parameters.

In deep learning regression applications, a big challenge is that limited training samples were presented for remote sensing due to labor-intensive and time-consuming field sampling. Ercanlı [59] predicted tree height-diameter relationships using deep learning regression models at the individual-tree level. The deep learning regression algorithm was fully connected network (FCN) that consisted of one input layer, many hidden layers, and one output layer. Despite the acceptable modeling accuracies obtained, the author found that one of the shortcomings of the study was the limitation of training sample size. Liu *et al.* [60] reviewed that the limitation of the future expansion of forest ecology research was the lack of available and suitable training samples. There have emerged relevant studies in the image processing field for small sample issues [61]–[63]. Wang and Hebert (2016) [64] have committed to solving small sample learning based on model regression networks. Considering the realistic need, the motivation in this article is to address the balance of deep learning regression efficiency and the number of training samples.

In this article, we developed the deep learning regression algorithm (called "Deep-RBN") with limited training samples to promote accurate forest structural parameter estimations. The algorithm integrated FCN regression algorithm as a basic deep regressor framework, with the modified radial basis neural network (RBN) algorithm as parameter preoptimizer. The modified RBN algorithm was designed by a multistep training process to undertake the first approximation procedure, and autoprecalculate the respective parameters of RBN layer. The RBN layer was the first hidden layer that consisted of radial basis function (RBF) neurons. Further approximation procedure was realized through autoweight optimization of FCN. Finally, several key forest structural parameters were predicted under two-stage approximation procedure using airborne LiDAR data by the Deep-RBN algorithm and assessed with filed data.

The main contributions of this article are as follows.

1) Develop the Deep-RBN deep learning regression algorithm and test the accuracy for limited training samples. By combining the FCN regressor with RBN parameter preoptimizer to learn deep features for forest structural parameter estimation.
2) Assess the efficiency and capability of the Deep-RBN algorithm in the key forest structural parameter estimation by combining with the FCN regression algorithm and classical regression algorithm (MLR).
3) Tune the hyperparameters of Deep-RBN and test its sensitivity under different numbers of training samples, terrain, and tree species. The optimized hyperparameter setting and practical training samples number were given for foresters to support EFIs.

II. Materials and Methods

A. Study Area

The study area is situated in Gaofeng Forest, located in the middle of Nanning city of Guangxi Province in southern

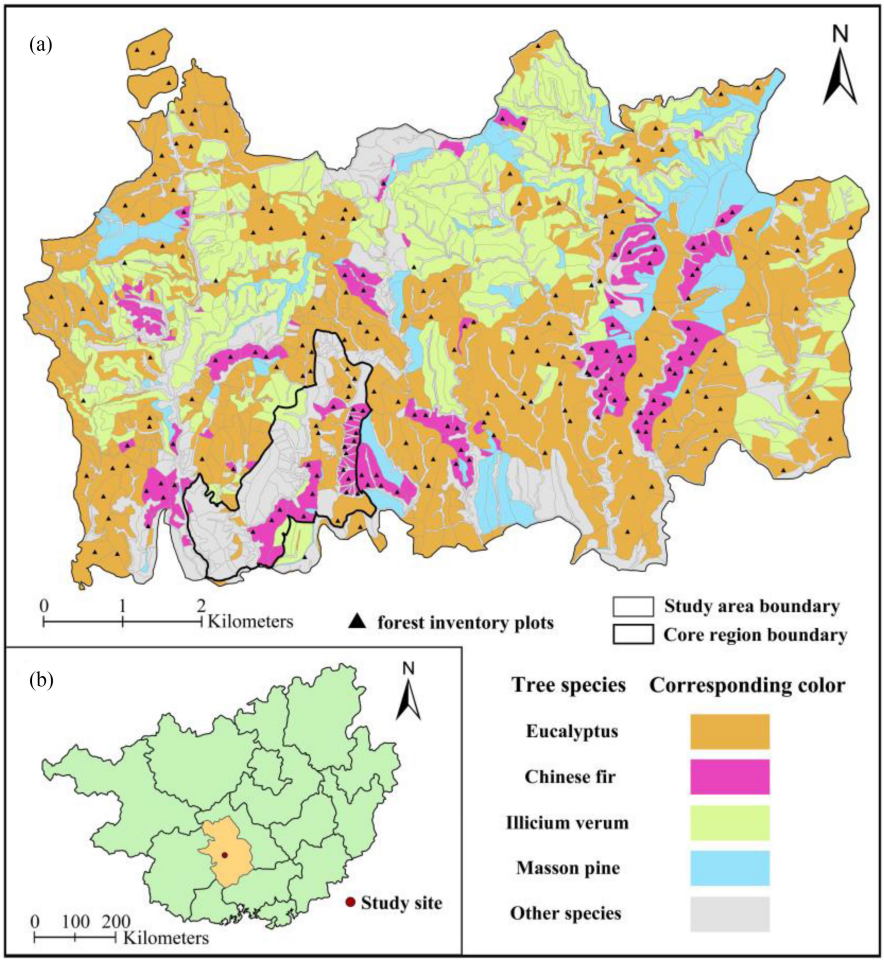

Fig. 1. Location of study area and field inventory plots with two main tree species (Eucalypt and Chinese fir). (a) Distribution of different tree species with specified colors. (b) Location of Guangxi Province in China.

China (22°49′–23°5′ N, 108°7′–108°38′ E) and covers approximately 5200 ha [see Fig. 1(a)]. It located in the subtropical monsoon climatic zone with the annual average temperature and precipitation of the study area are 21.6 °C and 1304 mm, respectively, and an elevation range 80–460 m above sea level. There is plenty of sunshine and rain with little frost and snow. The forest soil is mainly red soil, and the average thickness of the soil layer is above 80 cm. The main tree species in the area are Eucalypt (*Eucalyptus robusta Smith*) and Chinese fir [*Cunninghamia lanceolata* (Lamb.) Hook.]. Other species include Masson pine (Pinus massoniana Lamb.), Illicium verum (Illicium verum Hook.f.), Manglietia glauca (*Manglietia glauca* Blume), and acacia crassicarpa (*Acacia crassicarpa* Benth.). Within the study area, a core region was outlined according to historical survey data for further research. And, different tree species with specified colors were described in Fig. 1.

B. Forest Inventory Data

Between 16 January and 3 February 2018, a total of 49 square sample plots which are mainly composed of Eucalypt and Chinese fir (20 × 20 m) within the study area were established and measured. The coordinates of plot center were positioned by Trimble Juno T41/5 Handheld GPS instrument (Trimble, Sunnyvale, CA, USA). For all live trees within each plot, tree species, diameter at breast height (DBH) (using a diameter tape), tree height (using Vertex IV hypsometer), tree crown (using tape), and stand density were recorded with DBH larger than 5 cm.

To test the effect of the number of samples in the performance of deep learning algorithm, additional sample plots are needed in the analysis. According to the field measured tree species and historical survey data, 191 additional square plots in the eucalyptus and Chinese fir dominant stands were extracted, following the principle of random sampling, resulting in a total of 240 forest inventory plots. We used the normalized LiDAR data to extract 20 × 20 m square sample plots. Then, the individual trees were detected using a point cloud segmentation (PCS) algorithm [65]. Tree numbers and each individual tree height of each LiDAR plot were generated. Tree species specified DBH-height models were derived to obtain DBH for all trees [66]. The individual tree-level volume was calculated by the local species-specific volume equations according to forest inventory DBH and height, and then, summed into plot-level volume. A summary of forest inventory parameters was shown in Table I.

TABLE I
SUMMARY OF FOREST INVENTORY PARAMETERS

Forest structural parameters	Eucalyptus plots (± SD)	Chinese fir plots (± SD)
DBH (cm)	15.25±2.99	17.41±3.23
H (m)	17.51±3.53	15.20±2.56
V ($m^3 \cdot ha^{-1}$)	146.22±66.24	141.93±38.41
D ($n \cdot ha^{-1}$)	973±490	906±323

Notes: DBH = mean diameter at breast height; H = mean height; V = volume; D = stem density; SD = standard deviation.

TABLE II
AIRBORNE LIDAR DATA ACQUISITION PARAMETERS

Acquisition parameters	Description
Laser sensor	Rigel LMS-Q680i
Aircraft Speed	180 km/h
Flight altitude	750 m
Swath width	402 m
Max scan angle	30°
Beam divergence	0.5 mrad
Wavelength	1550 nm
Overlap	65%
Pulse Repetition Rate	300 kHz
Scan Frequency	80 Hz
Number of Returns Per Pulse	Fullwaveform-derived
Point Density	9.58 ts/m^2

C. LiDAR Data Acquisition and Preprocessing

Airborne LiDAR data were acquired in January 2018 using a Rigel LMS-Q680i system at an altitude of 750 m above ground level with a speed of 180 km/h (detailed flight parameters were shown in Table II). The average point density was 9.58 pts/m^2. LiDAR point clouds were stored in LAS 1.2 format (American Society for Photogrammetry and Remote Sensing, Bethesda, MD, USA).

During the preprocessing procedure, LiDAR point clouds were processed using the LiDAR360 software (GreenValley International, California, CA, USA). The ground and nonground returns were classified by the improved progressive triangulated irregular network (TIN) densification (IPTD) filtering algorithm developed by Zhao *et al.* [67]. The ground returns were interpolated using the inverse distance weighting (IDW) algorithm, resulting in a digital terrain model (DTM) with a resolution of 1 m. The heights of LiDAR returns were then normalized by the DTM to generate normalized point clouds. Finally, plot-level normalized point clouds were extracted by the boundary of field plots.

D. LiDAR Metrics Extraction and Selection

Plot-level LiDAR metrics were calculated from normalized point clouds, including height-related metrics and density-related metrics. Height-related metrics were extracted to represent the height of returns within the canopy, following the approach of [68]. In order to describe the distribution of point density, LiDAR returns were divided into ten slices with the same height interval from base to top height. Canopy return density metrics were finally generated by calculating the proportion of returns in each height interval. These specific LiDAR metrics were chosen as candidate input data for their ability to describe forest structural structures, including horizontal and vertical distribution of vegetation canopy. Typically, heighted-based metrics were generated to characterize vertical distribution of canopy elements. Density-based metrics were generated to describe horizontal canopy heterogeneity. In a combination of heighted-based and density-based metrics, 3-D structure of the forest stand was completely characterized as the form of metrics. The use of meaningful metrics as input helped strengthen the explaining ability of Deep-RBN. Besides, to remove the effect of ground and low vegetation [17], all LiDAR metrics were extracted above 2 m height threshold (see Table III).

E. Deep Learning Regressor

In this study, we developed a novel deep learning-based regression algorithm for estimating forest structural parameters, called "Deep-RBN." In order to assess the efficiency and capability of the Deep-RBN algorithm, the conventional FCN deep learning regression algorithm was added to compare the estimation accuracy of key forest structural parameters. Besides, the FCN algorithm was also used to be the basic architecture of the Deep-RBN algorithm.

The Deep-RBN algorithm combined the conventional FCN deep learning regression framework with the optimized radial basis network algorithm (RBN), considering the ability of autoweight optimization of deep learning, through multiple iterations, to constantly update the internal weights to achieve the optimization accuracy of model fitting, and also considering the advantages of optimized RBN algorithm that model accurately regresses with reduced training samples.

The RBN was a shallow layer neural network made up of a three-layer network (i.e., one input layer, one hidden layer, and one output layer), suitable for handling regression problems [69]. The RBN had the advantage of universal approximation to avoid local minima issues that produce inaccurate results [70]. The RBN used radial basis transfer functions (RBF) [71], commonly Gaussian kernel function, including two parameter basis functions center ($\boldsymbol{C}$) and spread (σ). However, traditional RBN usually had the overfitting issue which was primarily mitigated by setting a basis function center and spread [72]. Bataineh and Marler (2017) designed an optimized RBN algorithm (Opt-RBN) that used a modified orthogonal least squares (OLS) algorithm to optimize the setting of center ($\boldsymbol{C}$) and spread (σ) parameters. At the same time, a multistep training process was used to conduct the OLS algorithm and gradient-based optimization. It was especially proposed to handle the regression problems with limited training samples.

In this study, the RBN layer was set to be the first hidden layer that consisted of RBF neurons. The optimized RBN algorithm was further modified to undertake the first approximation procedure and autoprecalculate the respective parameters of RBN

TABLE III
LIDAR METRICS EXTRACTED FROM NORMALIZED POINT CLOUDS FOR ESTIMATING FOREST STRUCTURAL PARAMETERS

LiDAR metrics	**Description**
Percentile heights (H_{25}, H_{50}, H_{75}, H_{95})	The percentiles of canopy height distributions (25th, 50th, 75th, and 95th) > 2 m
Max height (H_{max})	Max of point heights > 2 m
Minimum height (H_{min})	Min of point heights > 2 m
Mean height (H_{mean})	Average of point heights > 2 m
Coefficient of variation of heights (H_{cv})	Coefficient of variation of point heights >2 m
Canopy return density (D_3, D_5, D_7, D_9)	The proportion of points in each height interval (30, 50, 70 and 90) >2 m (10th, 30th, 50th, 70th and 90th) to total number

TABLE IV
COMPARISON OF ACCURACY AND COMPUTING EFFICIENCY USING DIFFERENT FOREST STRUCTURAL PARAMETER REGRESSION ALGORITHMS

Forest structural parameters	Regression algorithms	R^2	RMSE	rRMSE	MAE	Run time (s)
Mean DBH	MLR	0.62	2.20	13.41	1.73	67
	FCN	0.65	2.94	17.98	2.36	139
	Deep-RBN	0.67	2.46	15.04	2.14	143
Mean height	MLR	0.76	1.33	8.32	1.01	50
	FCN	0.81	1.33	8.27	0.96	143
	Deep-RBN	0.86	1.12	6.95	0.90	149
Volume	MLR	0.58	28.72	21.34	20.21	43
	FCN	0.58	26.07	19.37	19.69	135
	Deep-RBN	0.73	19.45	14.45	15.19	169
Stem density	MLR	0.52	292.20	31.03	228.09	45
	FCN	0.61	291.88	30.99	187.89	133
	Deep-RBN	0.72	191.52	20.34	141.82	195

layer [i.e., center ($\boldsymbol{C}$) and spread (σ)]. Finally, the Deep-RBN algorithm was generated in the FCN deep learning framework to estimate forest structural parameters with limited training samples.

1) FCN Algorithm: We applied the FCN algorithm in Keras deep learning framework [73], written in Python on top of TensorFlow [74]. We trained the network with sequential model and used the adaptive moment estimation (Adam) optimizer [75], [76] to optimize neural networks. A total of five deep hidden layers were structured in the architecture. In the network, the rectified linear unit (ReLU) activation function was used to improve neural networks [77]. The dropout regularization was applied in the networks to avoid the overfitting problem [78]. In the sequential model, the dropout layer was inserted and a dropout rate of 0.2 was set at the same time. The batch size was set to 100. The learning rate was set to 0.001 and decay was 1e-4. In the FCN models, five hidden layers were set and five different neuron alternatives ranged from 100 to 20 by decreasing 20 at each step.

Based on the deep learning framework, the FCN algorithm was finally designed for comparing the estimation accuracy of key forest structural parameters with the Deep-RBN algorithm.

2) Deep-RBN Algorithm: The framework of the Deep-RBN algorithm was shown in Fig. 2. First, LiDAR metrics (see Table III) of each LiDAR plot were extracted as input data. Second, all m input neurons were fully interconnected to hidden layers. The RBN layer was used to convert input data with RBF activation function. Each RBF neuron with respective parameters (center $\boldsymbol{C}_i$ and spread σ_i) enabled the first optimal approximation to true values. After the RBN processing, converted data were put into deep learning framework that consisted of many deep layers with k hidden neurons and predesigned hyperparameters (i.e., optimizer, activation function, dropout, learning rate, and epochs) that were mentioned in the previous section of FCN algorithm. Further approximation procedure was realized through autoweight optimization of FCN. Finally, estimated forest parameters were calculated by two-stage approximation procedure and this enabled the regression accuracy with limited training samples.

In the Deep-RBN algorithm, the RBN layer was the first hidden layer that consisted of RBF neurons to undertake the first approximation procedure to true values. Each RBF neuron had the respective parameters that needed to be autoprecalculated by the independent calculation procedure. In the parameter calculation procedure, a three-layer (i.e., one input layer, one hidden layer, and one output layer) RBN network was built to train the network and obtain the best model approximation accuracy between input data and true values. According to the advantages of the Opt-RBN algorithm [72], a modified OLS algorithm and multistep training process were retained for automatic selection of RBF parameters.

In the RBN layer, each RBF neuron produced an activation function to transfer one input vector $\boldsymbol{x} = (x_1, x_2, \ldots, x_m)$ (m: number of LiDAR metrics) to each of the mth neuron output scalar h_i. The activation function was responsible to convert the relationship between the upper neuron output and the lower neuron input. The Gaussian kernel function was typically chosen

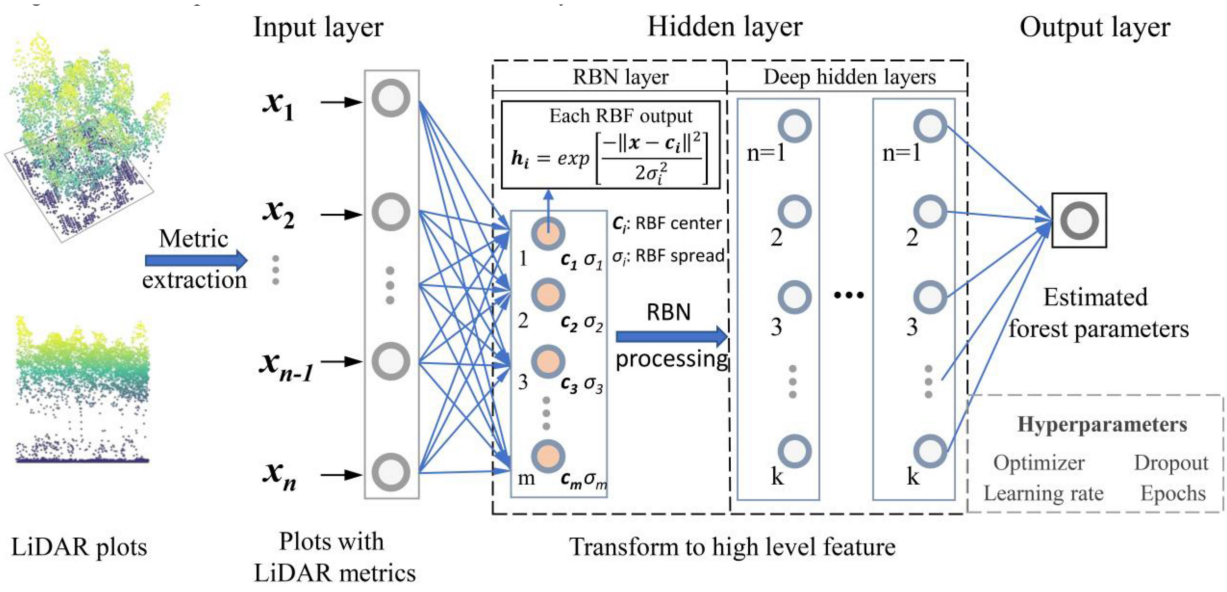

Fig. 2. Architecture of Deep-RBN algorithm. The LiDAR-derived metrics were added as input data, RBN layer, and multideep layers were consistent of hidden layer where multihyperparameters were added, estimated forest parameters values were output values.

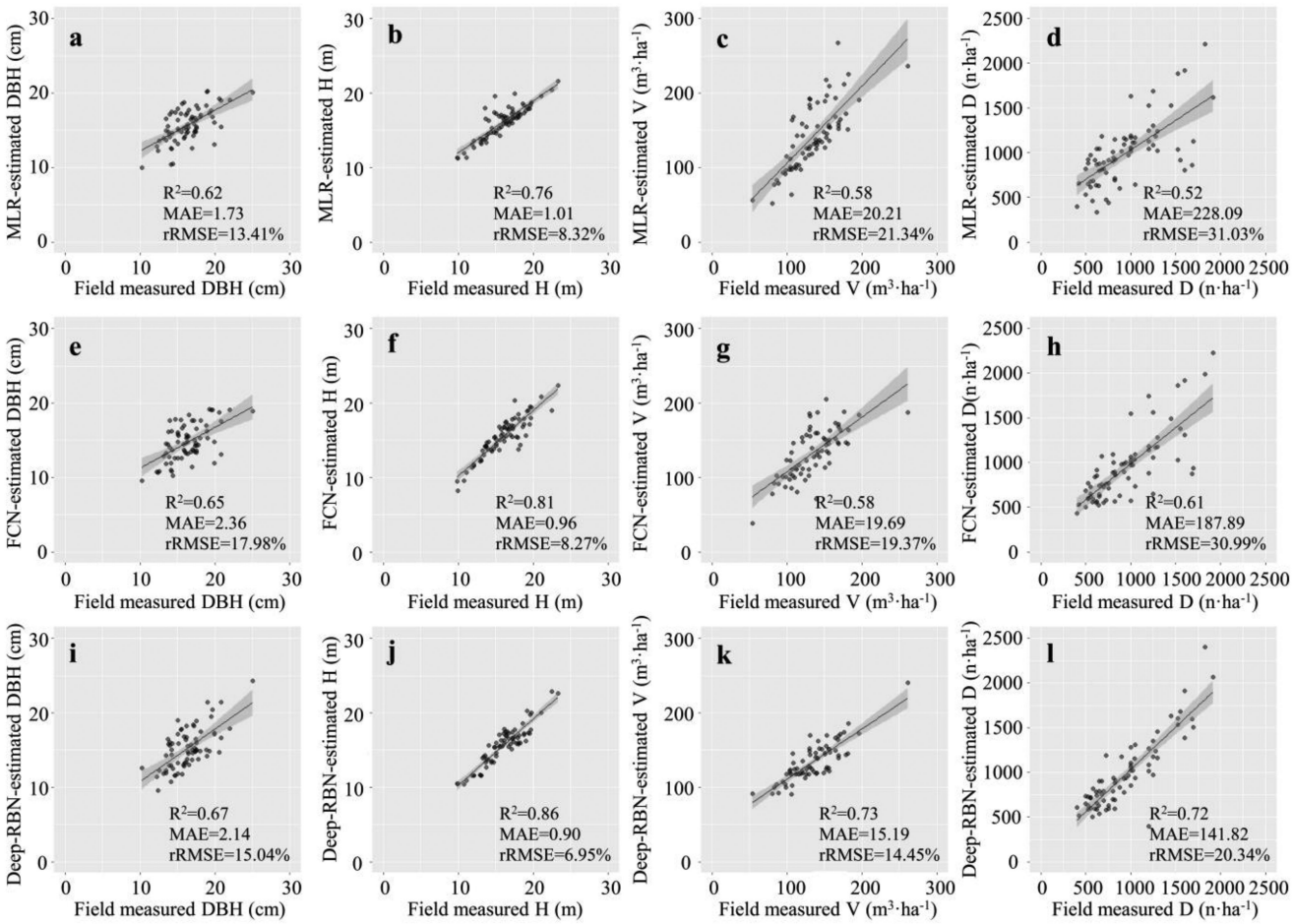

Fig. 3. Scatterplots of forest inventory values and model predicted mean DBH, mean height (H), volume (V), and stem density (D). (a)–(d) MLR-based results. (e)–(h) FCN-based results. (i)–(l) Deep-RBN-based results.

as basis function, the specific formula was as follows:

$$h_i = \exp\left[\frac{-\|\boldsymbol{x} - \boldsymbol{c_i}\|^2}{2\sigma_i^2}\right],\ i\ =\ 1, 2, \ldots, m \tag{1}$$

Where $\mathbf{c_i}$ and σ_i were the center and spread of Gaussian function of the *i*th hidden neuron, respectively. $\boldsymbol{c_i} = (c_1, c_2, \ldots, c_m)$ for *i*th hidden neuron, h_i was *i*th neuron's output.

Thus, *n*-dimensional input samples (*n*: number of training samples, i.e., LiDAR plots number) were then converted by the *i*th neuron to vector $\boldsymbol{h_i} = (h_{i1}, h_{i2}, \ldots, h_{in})$. Here, the number of RBF neurons was set equal to the number of LiDAR metrics.

The *i*th hidden neuron of the RBN layer was interconnected with the *j*th output neuron $\boldsymbol{y_j}$ by the weighting factor w_{ij}. The output neuron $\boldsymbol{y_j}$ was then transferred to deep hidden layers for further calculation. *j* is an index of *k*.

$$\boldsymbol{y_j} = \boldsymbol{h_j}\ \cdot\ \mathbf{w_j} = \sum_{i=1}^{m} \boldsymbol{h_{ij}} \cdot\ w_{ij},\ j\ =\ 1,\ 2,\ \ldots,\ k. \tag{2}$$

In the multistep training process, the selection of basis function parameters $\boldsymbol{c}$ and σ was mainly to be optimized. The spread σ_i represented the width of each RBF neuron and the setting of spread impacted the network accuracy. In the calculation of the RBF spread, the spread σ_i of *i*th RBF was identified based on (3), which determined the Euclidean distance between each RBF center $\boldsymbol{C_i}$ and its nearest center $\boldsymbol{C_h}$. Herein, $\boldsymbol{C}_i$ was equal to the *i*th input training sample. *n* is number of training samples

$$\sigma_i = \ \mathrm{RMSD}\ = \sqrt{\sum\nolimits_{I=1}^{n} \left(\boldsymbol{C_i} - \boldsymbol{C}_h\right)^2}\ ,\ 1 \le i \le n. \tag{3}$$

In the calculation of the RBF center, it was determined by the modified OLS algorithm. In the *q*th iteration process, all previous $q-1$ basis function outputs $\boldsymbol{h}_{q\text{-}1}$ were used to calculate the orthogonal matrix based on QR-decomposition [79]. $\boldsymbol{Q}$ was an orthogonal matrix and an upper triangular matrix $\boldsymbol{R}$

$$\boldsymbol{H}\ =\ \boldsymbol{QR}. \tag{4}$$

The error reduction ratio $[\mathrm{err}]_i$ was generated to assess the importance of each training case for prediction error reduction. $\boldsymbol{t}$ represented the ground measured true values

$$[\mathrm{err}]_i = \frac{g_i^2 \boldsymbol{Q_i^T Q_i}}{\boldsymbol{t^T t}} \tag{5}$$

$$g_i = \left(\boldsymbol{Q_i^T}\ \boldsymbol{t}\right)/\left(\boldsymbol{Q_i^T Q_i}\right). \tag{6}$$

Thus, we acquired each RBF center $\boldsymbol{C}_i$ by detecting the highest $[\mathrm{err}]$ of the corresponding training samples. Each RBF spread was calculated by (3). The RBN hidden layer was generated with respective RBF center and spread of each neuron.

Now that the parameters of respective RBF center and spread of each neuron were calculated, each input vector $\boldsymbol{x} = (x_1, x_2, \ldots, x_n)$ was then converted to each of the *m* RBF neuron's output h_i. All *m* input vectors were thus converted to each of the *m* RBF neuron's output $\boldsymbol{h_i}$. All *m* input vectors were then converted to *m* RBF neuron's output matrix $\boldsymbol{H} = [\boldsymbol{h_1}, \boldsymbol{h_2}, \ldots, \boldsymbol{h_m}]$. The matrix $\boldsymbol{H}$ was then transferred to deep hidden layers for further deep learning procedure.

When considering deep learning framework, we used the FCN algorithm as the basic architecture of Deep-RBN. The FCN algorithm used an FCN structure with many hidden layers and had the advantage of easy-use in Keras. It learned features from array or matrix, which resulted in fast speed. Nevertheless, point-based framework extracted features from raw point cloud that may consume computing time, resulting in low efficiency. Proceeding from these backgrounds, the FCN algorithm was selected as the basic architecture of Deep-RBN.

In the Deep-RBN neural network, the activation function is a functional relationship that is responsible for converting the relationship between the output of the upper node and the input of the lower node. The ReLU function is popular in the neural network for its advantages, i.e., computational simplicity, representational sparsity, linear behavior. The function changes all negative values to zero while the positive values remain unchanged. The characteristics of unilateral inhibition make the neurons in neural networks sparsely activated. It solves the problem of gradient disappearance, provides higher sensitivity for activation sum input, and avoids easy saturation. Besides, the sparse model realized by ReLU can better mine relevant features and fit training data. The specific mathematical formula is as follows:

$$f\ (x) = \max(0, x). \tag{7}$$

The choice of the optimization algorithm may affect the difference of accuracy and efficiency of the deep learning model. When adjusting the model update internal parameters (weight and bias), the appropriate optimization algorithm can improve the training model, making the model converge better and faster. Adam is a stochastic gradient descent algorithm based on first-order moment and second-order moment of the gradient to update network weights. This optimizer combines the optimal performance of the AdaGrad and RMSProp algorithms and it provides an optimization method for solving sparse gradients and noise problems. Compared with other adaptive learning rate algorithms, its convergence speed is faster and the learning effect is more effective, and it can correct the problems existing in other optimization techniques, such as the disappearance of learning rate, the slow convergence, or the large fluctuation of loss function caused by the updating of high variance parameters. The specific mathematical formulas of Adam are as follows:

$$m_t = \beta_1\ \times m_{t-1} + (1 - \beta_1) \times g_t \tag{8}$$

$$n_t = \beta_2\ \times n_{t-1} + (1 - \beta_2) \times g_t^2 \tag{9}$$

$$\hat{m}_t = \frac{m_t}{1 - \beta_1^t} \tag{10}$$

$$\hat{n}_t = \frac{n_t}{1 - \beta_2^t} \tag{11}$$

$$\theta_{t+1} = \theta_t\ - \alpha \times \frac{\hat{m}_t}{\sqrt{\hat{n}_t} + \delta} \tag{12}$$

where g_t is gradient descent function on iteration t, m_t is biased first-order moment estimate of gradient g_t, n_t is biased second-order raw moment estimate of gradient g_t, β_1 is first-order moment attenuation coefficient, β_2 is second-order moment attenuation coefficient, $\hat{m}_t$ is bias-corrected first-order moment estimate for m_t, $\hat{n}_t$ is biased second-order raw moment estimate for n_t, θ_t is network parameters on iteration t, α is learning rate which controls stepsize, δ is a constant created for

numerical stability, and θ_{t+1} is pending update parameters on iteration $t+1$.

In the deep hidden layers, we set the same parameter architecture with the FCN algorithm, i.e., five hidden layers with five different neuron alternatives ranged from 100 to 20 by decreasing 20 at each step. k was 100 for the first hidden layer of deep hidden layers, 80 for the second layer, 60 for the third layer, 40 for the fourth layer, and 20 for the fifth layer. The neurons architecture of the whole Deep-RBN was n-m-100-80-60-40-20-1. The output neuron number was 1. The hyperparameter setting was the same with the FCN algorithm.

F. Traditional Regressor

Due to the advantage of easy understanding and widespread application for developing predictive models, multiple linear regression (MLR) was used in this study to estimate forest structural parameters. The forward stepwise modeling approach was used to build regression models that the selected LiDAR metrics and field data as input. All regression analyses were conducted in MATLAB R2016b (The MathWorks Inc., Natick, MA, USA).

G. Model Evaluation and Accuracy Assessment

We estimated four key forest structural parameters (mean DBH, mean height, volume, and stem density) by the statistical model (MLR), FCN model (FCN), and deep learning-based model (Deep-RBN) in this study, respectively. All plots were split into training set and test set according to the ratio of 7:3. The performance of predictive models was evaluated by the coefficient of determination (R^2), root-mean-square error (RMSE), relative RMSE (rRMSE), and mean absolute error (MAE).

$$R^2 = 1 - \frac{\sum_{i=1}^{n}(x_i - \hat{x}_i)^2}{\sum_{i=1}^{n}(x_i - \overline{x}_i)^2} \tag{13}$$

$$\mathrm{RMSE} = \sqrt{\frac{1}{n}\sum_{i=1}^{n}(x_i - \hat{x}_i)^2} \tag{14}$$

$$\mathrm{rRMSE} = \frac{\mathrm{RMSE}}{\bar{x}} \times 100\% \tag{15}$$

$$\mathrm{MAE} = \frac{1}{n}\sum_{i=1}^{n}|x_i - \hat{x}_i| \tag{16}$$

where x_i represents measured value; $\overline{x_i}$ is the average measured value; $\hat{x}_i$ is the estimated value; $\bar{x}$ is the mean field measured values; p is the number of LiDAR metrics; i is the plot number; n is the number of plots.

III. Results

A. Accuracy Assessment Using Different Modeling Algorithms

In order to assess the ability of deep learning regressor (Deep-RBN), different modeling algorithms (i.e., MLR, FCN, and Deep-RBN) were tested and compared with the predictive accuracy in estimating four key forest structural parameters.

The accuracy assessment results of three predictive methods showed that Deep-RBN had the highest accuracy (R^2 = 0.67–0.86, rRMSE = 6.95%–20.34%) within the three modeling algorithms (Table IV). FCN had a relatively lower accuracy (R^2 = 0.58–0.81, rRMSE = 8.27%–30.99%) than Deep-RBN. MLR had the lowest accuracy (R^2 = 0.52–0.76, rRMSE = 8.32%–31.03%). For forest structural parameters, mean height had the highest accuracy (R^2 = 0.76–0.86, rRMSE = 6.95%–8.32%), followed by DBH (R^2 = 0.62–0.67, rRMSE = 13.4%–17.98%) and volume (R^2 = 0.58–0.73, rRMSE = 14.45%–21.34%), stem density had the lowest accuracy (R^2 = 0.52–0.72, rRMSE = 20.34%–31.03%).

B. Mapping Results Assessment Using Different Modeling Algorithms

Accuracy and detailed mapping for key forest structural parameters are essential for characterizing forest composites and structure, and supporting forest decisions. The core region (see Fig. 1) within the study area was especially extracted to compare the detailed mapping results using MLR, FCN, and Deep-RBN methods (see Fig. 4). The nonforest (road, building, and water) cells were masked to eliminate the impact. Eucalypt and Chinese fir (field measured tree species) stand were retained to compare the forest structural parameter mapping results. The first column was MLR, the second column was FCN, the third column was Deep-RBN. Overall, MLR, FCN, and Deep-RBN had similar estimation values. For a-3, Deep-RBN detected detailed information, which represented accurate values of forest parameters. For subfigures of b-3, c-3, d-3, Deep-RBN represented more variation, which characterized the greater difference within forest stands. In conclusion, the Deep-RBN algorithm had a strong capacity to characterize the detailed forest structural information.

C. Spatial Extrapolation of Forest Structural Parameters Using Deep-RBN Models

Wall-to-wall mapping of study area was generated by Deep-RBN models. Eucalypt and Chinese fir stand were used to show forest structural parameter mapping results. Fig. 5 represented the spatial extrapolation results of forest structural parameters, which indicated the spatial distribution of DBH, mean height, volume, and stem density. Forest attribute maps ranged from blue to red, which represented the values. It was indicated that forest structural parameters had specific and related spatial distribution patterns.

D. Hyperparameter Tuning of Deep-RBN Models

Determining the optimal structure and parameter settings of the Deep-RBN model was critical for optimizing the model prediction results and improving the computational efficiency [80]. Hyperparameters determined the neural network structure (e.g., number of layers and neurons) and the training algorithm (e.g., learning rate and epoch number) [81]. It was helpful to tailor the behavior of deep learning algorithms to the given dataset.

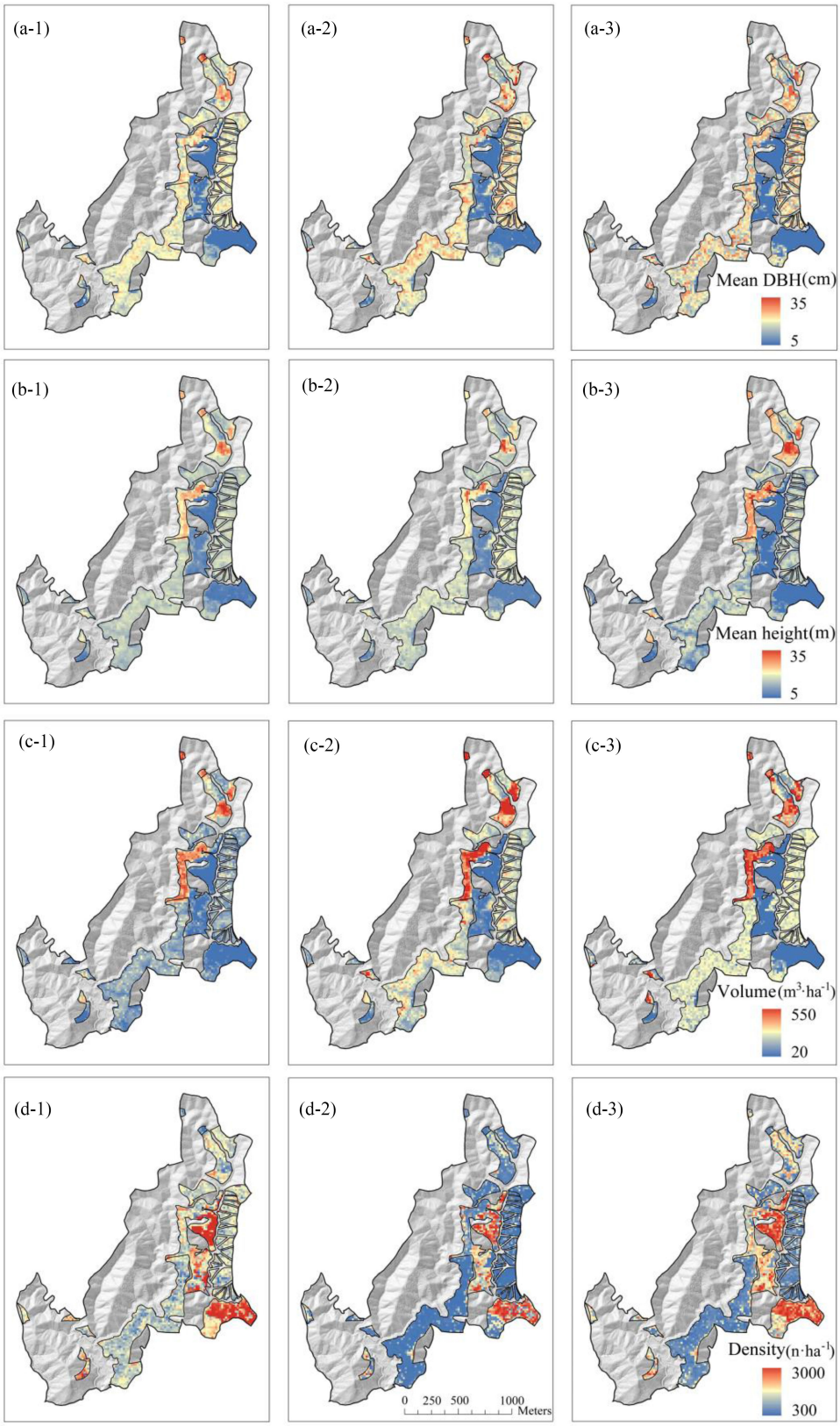

Fig. 4. Mapping result comparison using MLR, FCN, and Deep-RBN for forest structural parameters in the core region, i.e., (a-1, a-2, a-3) mean DBH, (b-1, b-2, b-3) mean height, (c-1, c-2, c-3) volume, and (d-1, d-2, d-3) stem density. MLR: a-1, b-1, c-1, d-1; FCN: a-2, b-2, c-2, d-2; Deep-RBN: a-3, b-3, c-3, d-3.

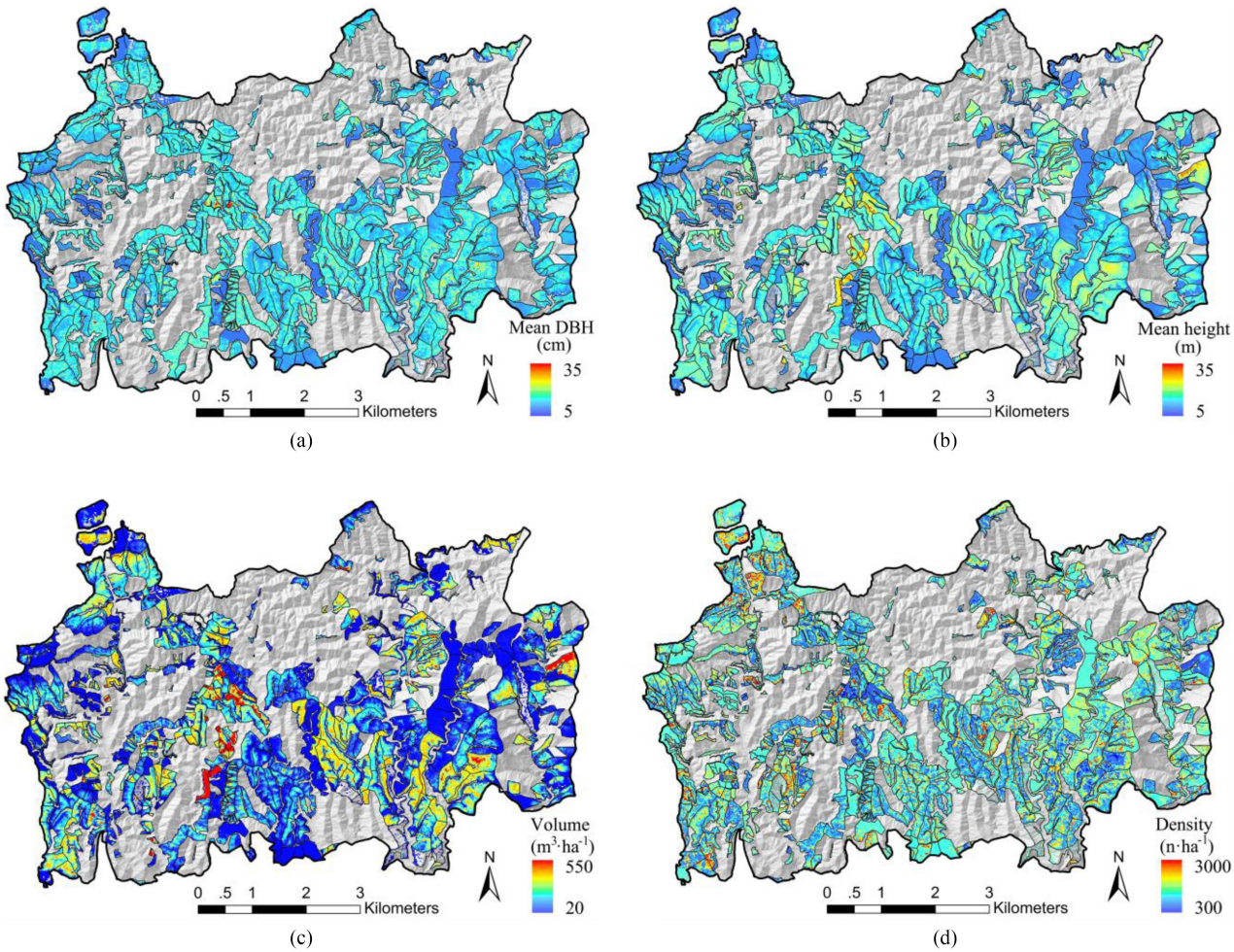

Fig. 5. Spatial extrapolation of forest structural parameters using Deep-RBN models. (a) Mean DBH. (b) Mean height. (c) Volume. (d) Stem density.

However, excessive hyperparameters may have a negative impact on the tuning process and model performance consistency. Thus, we tuned the learning rate and epoch number in this study to choose the best configuration of Deep-RBN models.

Learning rate (Lr) was a key hyperparameter that controlled how quickly the neural network updates its parameters in response to the estimated error. It was a challenging work to choose optimal Lr when configuring the neural network. When the learning rate was too large, the model may not converge, resulting in an unstable training process; if the learning rate was too small, the convergence speed of the model will be slow, which required longer training time. Usually, the Lr value was 0.01, 0.001, 0.0001. Herein, we test these three Lr values for estimating forest structural parameters. The epoch that defined how many times the neural network trained was set as 20 000 so that we could find a stable time of model training.

In Fig. 6, the curve represented relative mean squared error (RMSE) loss over training epochs. The values of RMSE under different Lr were given out (epoch = 10 000). For all forest structural parameters, it was indicated that Lr = 0.001 (blue curve) was the best choice for the Deep-RBN in this study because it acquired the lowest error and the most stable condition than the other two Lr values.

E. Influence of Training Sample Numbers on Deep-RBN Model Accuracy

Although deep learning algorithms have excellent performance with large samples, the behaviors may be restricted with reduced training samples for practical cost and labor limitations. Therefore, it was greatly significant to balance training case numbers and Deep-RBN model accuracy. Herein, we selected the optimized hyperparameters (i.e., Lr = 0.001) according to Fig. 6 and test the sensitivity of the number of training samples for Deep-RBN model results.

We selected training and test samples from all 240 samples and grouped them according to the scales of 70% training and 30% test samples. The number of training samples ranged from 20 to 160. Once, ten additional training samples were added to Deep-RBN models. Once the model was fitted, test cases were used to verify model accuracy (see Fig. 7). It was indicated that with the increase of training samples, the validation error

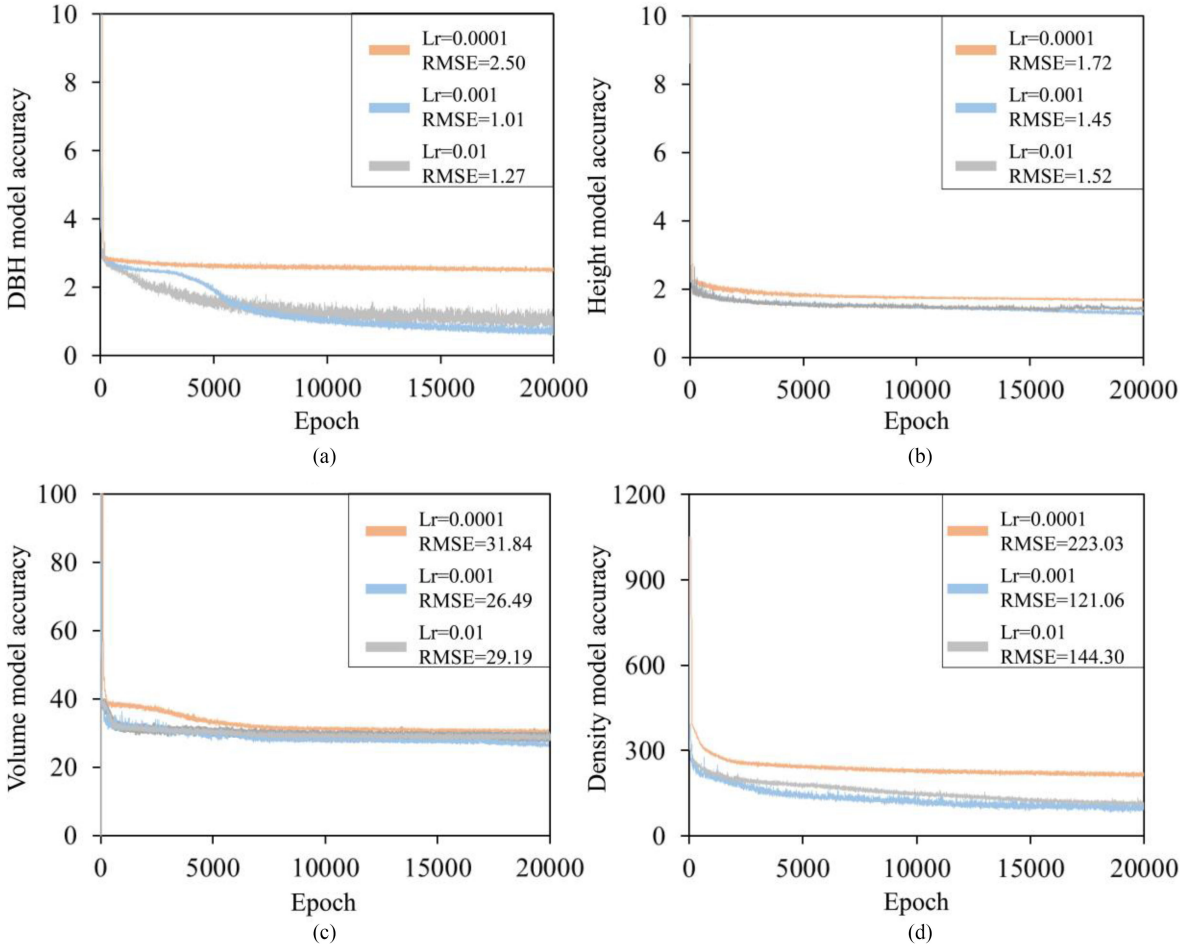

Fig. 6. Hyperparameter (learning rate and epoch number) tuning results comparison for predicting (a) DBH, (b) mean height, (c) volume, and (d) stem density. The curve represents relative mean squared error (RMSE) loss over training epochs. Orange, blue, and gray curves represent different learning rates of 0.0001, 0.001, and 0.01, respectively.

decreased. When training samples were larger than 70, the error of mean DBH, mean height, and volume were lower than 20%.

F. Influence of Other Factors on Deep-RBN Model Accuracy

In order to test the uncertainty of various forest structural parameters and the reliability of Deep-RBN algorithms, the influence of other factors was also considered, such as terrain and different tree species.

To test the influence of terrain, LiDAR-extracted DEM was used to calculate the slope of all plots. All plots were classified to low slope group that has the slope values between 0° and 30° and to high slope group that has the slope values between 30° and 60°. Next, in each group, 70% training samples were used to build forest structural parameter models, 30% test samples were used to verify the model accuracy. The Deep-RBN model results were shown in Table V. The difference of predictive accuracy (rRMSE) between low slope group (0°–30°) and high slope group (30°–60°) is 2.24% for mean DBH, 1.99% for mean height, 2.36% for volume, and 0.04% for stem density. Results showed the relative stable predictive accuracy (difference: 0.04%–2.36%).

TABLE V
ACCURACY (RRMSE) COMPARISON BETWEEN LOW SLOPE GROUP (0°–30°) AND HIGH SLOPE GROUP (30°–60°)

Slope	Forest structural parameters	RMSE	rRMSE (%)	MAE
Low slope (0°-30°)	Mean DBH	2.66	16.61	2.15
	Mean height	1.99	11.70	1.47
	Volume	27.51	17.75	20.76
	Stem density	199.50	21.26	148.46
High slope (30°-60°)	Mean DBH	2.29	14.37	1.82
	Mean height	1.62	9.71	1.27
	Volume	22.76	15.39	16.53
	Stem density	205.47	21.30	153.23

To test the influence of tree species, we test two main tree species (i.e., Eucalyptus and Chinese fir) into the Deep-RBN models. According to historical survey stand data of tree species, all plots are grouped as Eucalyptus group and Chinese fir group. Next, in each group, 70% training samples were used to build forest structural parameter models, 30% test samples were used to verify the model accuracy. The Deep-RBN model results were shown in Table VI. The difference of predictive accuracy (rRMSE) between Eucalyptus group and Chinese fir group is

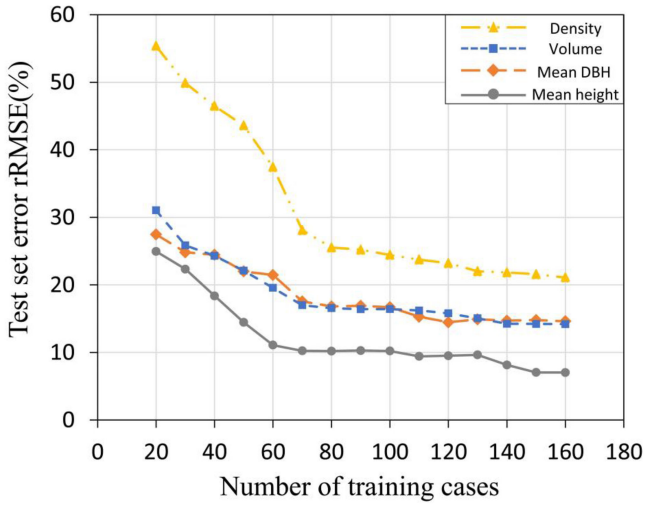

Fig. 7. Sensitivity of training sample numbers for Deep-RBN model results.

TABLE VI
ACCURACY (RRMSE) COMPARISON BETWEEN EUCALYPTUS GROUP AND CHINESE FIR GROUP

Tree species	Forest structural parameters	RMSE	rRMSE (%)	MAE
Eucalyptus	Mean DBH	2.05	13.46	1.63
	Mean height	1.87	10.72	1.46
	Volume	26.08	17.66	20.65
	Stem density	207.21	21.34	143.96
Chinese fir	Mean DBH	2.21	12.42	1.84
	Mean height	1.39	9.04	1.06
	Volume	22.03	14.53	17.88
	Stem density	177.83	19.87	151.27

1.04% for mean DBH, 1.68% for mean height, 3.13% for volume, and 1.47% for stem density. Results showed the relative stable predictive accuracy (difference: 1.04%–3.13%).

In summary, it was indicated that the estimated accuracy of Deep-RBN algorithm was relatively reliable and stable under different factor tests.

IV. DISCUSSION

A. Interpretation of Deep-RBN Models

In this study, the Deep-RBN algorithm was implemented in estimating forest structural parameters with the accurate estimations. Deep learning was able to generalize discrete and continuous data well and was little affected by the factors, such as terrain, tree species. [41]. Similar to common machine learning methods, deep learning was also known as the "black box." Although the model obtains optimal fitting results and mapping performance, it was of great significance to understand how Deep-RBN model worked and what knowledge would be learned. To interpret the predictive model, variable importance was used to determine the weight of each metric, which represented the relative importance within each Deep-RBN model (see Fig. 8). For Deep-RBN models, variable importance was calculated using Gedeon's method [82], which considered the weights of the data input to the first two hidden layers for its simplicity and efficiency [83].

According to the best predictive models, i.e., Deep-RBN models, the variable importance of each forest parameters was summarized (see Fig. 8). The relative importance of LiDAR metrics was related to the explanatory ability of each forest structural parameter. For DBH model, D_5, H_{skewness}, and H_{25} were the top three predictors. For mean height model, D_5, H_{25}, and H_{median} had the highest importance. For volume model, H_{25}, D_5, and H_{cv} contributed to approximately 13% of the importance. For density model, D_5, H_{cv}, and H_{skewness} had the highest importance values for model predictors.

B. Volume Distribution Mapping for Different Tree Species and Forest Types

As a basic unit in silvicultural practices, forest stand was the spatial subdivision region that has the steady and homogeneous characters, such as forest type, tree species, age class, site quality. Wall-to-wall forest parameter mapping in stand-level with Deep-RBN predictive model is beneficial for forestry applications, such as forestry management and silviculture.

Based on the mapping results, we extracted the stand-level volume distribution map of Eucalypt (E.Rob) and Chinese fir (C.Fir) stand, as well as the histogram of stand-level volume distribution statistics, which was important for understanding the current situation of forest management and future forest management.

Two tree species (i.e., E.Rob, C.Fir) with different forest types (i.e., species dominate forest and mixed forest) that exhibited typicality and representativeness in the study area were shown in Fig. 9. The stand boundary that is overlaid on the volume map clearly distinguished each subclass.

According to stand-level summary results, the volume distribution of E.Rob dominate forest, C.Fir dominate forest, E.Rob mixed forest, and C.Fir mixed forest were calculated and displayed in Fig. 9(b)–(e), respectively. Each volume class was set to $10\,\text{m}^3\cdot\text{ha}^{-1}$ and ranged from 0 to $300\,\text{m}^3\cdot\text{ha}^{-1}$. Proportions of each volume class indicated the condition of forest stands and difference of tree species and forest types. From the aspect of histogram shape, values distributed more evenly in each class in E.Rob forest and sharper in C.Fir forest. From the aspect of histogram peak value location, E.Rob dominate forest was about $100\,\text{m}^3\cdot\text{ha}^{-1}$, C.Fir dominate forest was about $130\,\text{m}^3\cdot\text{ha}^{-1}$, E.Rob mixed forest was about $140\,\text{m}^3\cdot\text{ha}^{-1}$, and C.Fir mixed forest was about $140\,\text{m}^3\cdot\text{ha}^{-1}$.

C. Advantages of the Deep-RBN Algorithm

The Deep-RBN algorithm was tested to assess its capability and efficiency with the FCN algorithm and MLR. It indicated that Deep-RBN had the highest accuracy and better performance for relatively small training samples. It benefited from the preprocessing of the optimized RBN algorithm and the framework of deep learning.

In the optimized RBN algorithm designed for reduced training sample regression, we retained a modified OLS algorithm and multistep training process. The optimized RBN algorithm helped to undertake the first approximation procedure between LiDAR metrics and the ground true values. At the same time,

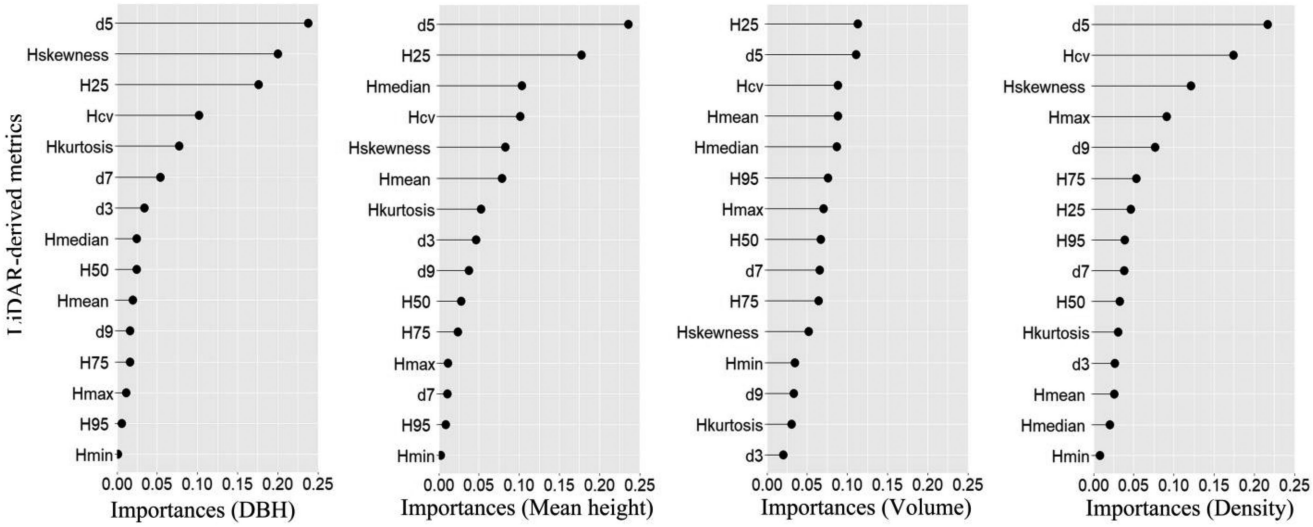

Fig. 8. Variable importance generated for each Deep-RBN model. The description of LiDAR-derived metrics was shown in Table III.

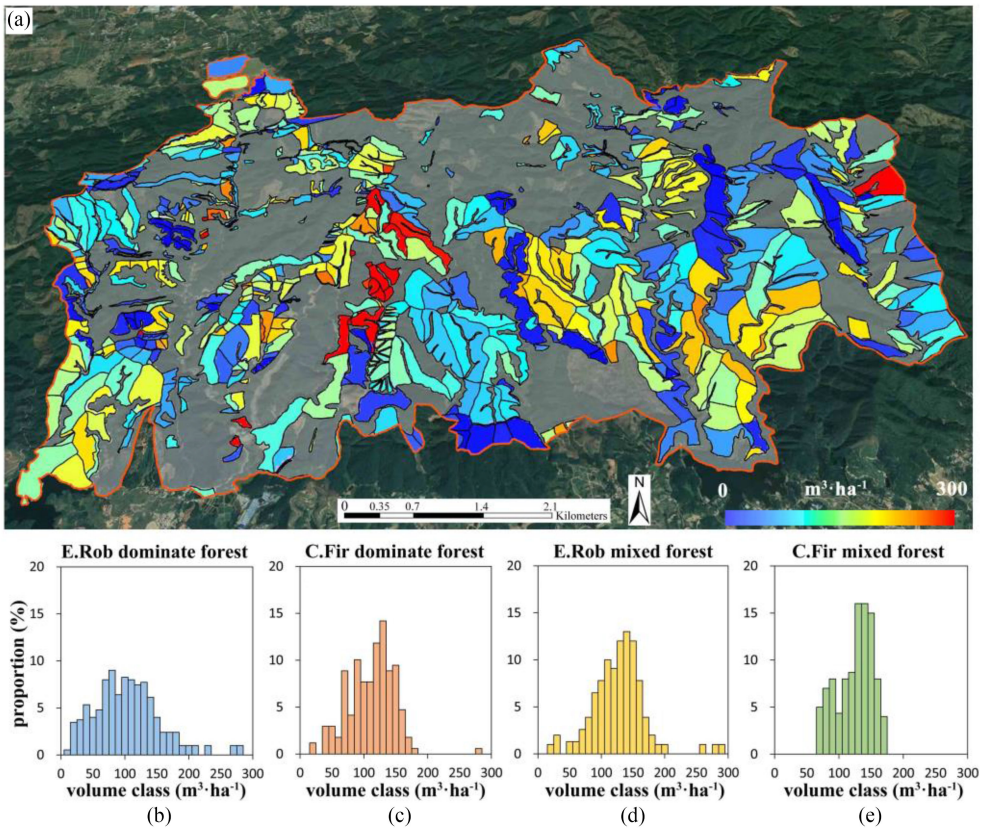

Fig. 9. Volume distribution of study area for two main tree species (i.e., Eucalyptus and Chinese fir) in different forest types (i.e., species dominate forest and mixed forest).

parameters of the RBN layer were automatically calculated for further processing. In the second approximation procedure, deep learning framework was used to undertake the autoweight optimization processing to improve the accuracy of the fitted model. Thus, a two-stage approximation procedure ensured the outstanding results of forest structural parameter estimation with limited training samples.

Besides, the deep learning-based regression algorithm may achieve better fitting models by tuning the hyperparameters. The results showed that along with the increasing training sample number, the models tended to have stably higher accuracy. It indicated that the tradeoff of the number of samples should be considered while applying the Deep-RBN algorithm in different forests which others could do.

V. Conclusion

This study demonstrated that the novel deep learning regression algorithm is a promising tool to use airborne LiDAR data to estimate and map forest structural parameters in the subtropical planted forest of southern China. The Deep-RBN algorithm had the advantages of the FCN algorithm with the optimized RBN algorithm. We found that it was suitable to estimate forest structural parameters with limited training samples. Through comparing the FCN algorithm with traditional regression algorithm, it indicated that the Deep-RBN algorithm obtained the highest accuracy of predictive models and the most detailed mapping information, which were essential for estimating forest parameters and monitoring forest resources at large scale. We found that it helped to improve the Deep-RBN algorithm by tuning the hyperparameters. Besides, the volume distribution of the volume map showed the various forest conditions of different tree species and forest types. This will help to observe the present situation of forest management more intuitively and provide the basis for future forest decision-making.

References

[1] H. Baral, M. Guariguata, and R. Keenan, "A proposed framework for assessing ecosystem goods and services from planted forests," *Ecosyst. Services*, vol. 22, Part B, pp. 260–268, Dec. 2016.

[2] J. W. Thomas, "Forest service perspective on ecosystem management," *Ecol. Appl.*, vol. 6, no. 3, pp. 703–705, 1996.

[3] N. Buchmann and J. Roy, "Species diversity, functional diversity and ecosystem functioning," *Biodivers. Ecosyst. Funct. Synth. Perspect.*, vol. 17, pp. 195–208, 2002.

[4] C. Messier and D. D. Kneeshaw, "Thinking and acting differently for sustainable management of the boreal forest," *For. Chron.*, vol. 75, no. 6, pp. 929–938, 1999.

[5] X. Wei and J. A. Blanco, "Significant increase in ecosystem C can be achieved with sustainable forest management in subtropical plantation forests," *PLoS One*, vol. 9, no. 2, 2014, Art. no. e89688.

[6] R. E. McRoberts, "The enhanced forest inventory and analysis program," U.S. Dep. Agric. For. Serv. South. Res. Station., Asheville, NC, USA, Gen. Tech. Rep. SRS-80., pp. 11–20, 2005.

[7] M. A. Wulder, C. W. Bater, N. C. Coops, T. Hilker, and J. C. White, "The role of LiDAR in sustainable forest management," *Forestry Chron.*, vol. 84, no. 6, pp. 807–826, 2008.

[8] J. C. White, N. C. Coops, M. A. Wulder, M. Vastaranta, T. Hilker, and P. Tompalski, "Remote sensing technologies for enhancing forest inventories: A review," *Can. J. Remote Sens.*, vol. 42, no. 5, pp. 619–641, 2016.

[9] T. R. H. Goodbody, N. C. Coops, T. Hermosilla, P. Tompalski, G. McCartney, and D. A. MacLean, "Digital aerial photogrammetry for assessing cumulative spruce budworm defoliation and enhancing forest inventories at a landscape-level," *ISPRS J. Photogramm. Remote Sens.*, vol. 142, no. Apr., pp. 1–11, 2018.

[10] W. A. Bechtold and P. L. Patterson, "The enhanced forest inventory and analysis program—National sampling design and estimation procedures," *USDA Forest Service, Southern Research Station*, vol. 80, 2005.

[11] A. T. Hudak *et al.*, "Quantifying aboveground forest carbon pools and fluxes from repeat LiDAR surveys," *Remote Sens. Environ.*, vol. 123, pp. 25–40, 2012.

[12] M. Woods *et al.*, "Operational implementation of a LiDAR inventory in Boreal Ontario," *Forestry Chron.*, vol. 87, no. 4, pp. 512–528, 2011.

[13] M. A. Lefsky, W. B. Cohen, G. G. Parker, and D. J. Harding, "Lidar remote sensing for ecosystem studies," *BioScience*, vol. 52, no. 1, pp. 19–30, 2002.

[14] M. A. Lefsky, W. B. Cohen, S. A. Acker, G. G. Parker, T. A. Spies, and D. Harding, "Lidar remote sensing of the canopy structure and biophysical properties of Douglas-fir western hemlock forests," *Remote Sens. Environ.*, vol. 70, no. 3, pp. 339–361, 1999.

[15] L. Cao *et al.*, "Estimation of forest biomass dynamics in subtropical forests using multi-temporal airborne LiDAR data," *Remote Sens. Environ.*, vol. 178, no. Jun., pp. 158–171, 2016.

[16] N. C. Coops *et al.*, "Estimating canopy structure of Douglas-fir forest stands from discrete-return LiDAR," *Trees, Struct. Funct.*, vol. 21, no. 3, pp. 295–310, 2007.

[17] J. C. White, A. Wulder, N. C. Coops, D. Cook, and D. Pitt, "A best practices guide for generating forest inventory attributes from airborne laser scanning data using an area-based approach," *For. Chron.*, vol. 89, no. 6, pp. 722–723, 2013.

[18] P. Liu, K. R. Choo, L. Wang, and F. Huang, "SVM or deep learning? A comparative study on remote sensing image classification," *Soft Comput.*, vol. 21, pp. 7053–7065, 2017.

[19] D. K. Bolton, N. C. Coops, and M. A. Wulder, "Characterizing residual structure and forest recovery following high-severity fire in the western boreal of Canada using Landsat time-series and airborne lidar data," *Remote Sens. Environ.*, vol. 163, pp. 48–60, 2015.

[20] J. E. Means, S. A. Acker, B. J. Fitt, M. Renslow, L. Emerson, and C. J. Hendrix, "Predicting forest stand characteristics with airborne scanning Lidar," *Photogramm. Eng. Remote Sensing*, vol. 66, no. 11, pp. 1367–1371, 2000.

[21] J. Holmgren, "Prediction of tree height, basal area and stem volume in forest stands using airborne laser scanning," *Scand. J. Forest Res.*, vol. 19, no. 6, pp. 543–553, 2004.

[22] E. Næsset *et al.*, "Model-assisted regional forest biomass estimation using LiDAR and InSAR as auxiliary data: A case study from a boreal forest area," *Remote Sens. Environ.*, vol. 115, no. 12, pp. 3599–3614, 2011.

[23] M. Vastaranta, V. Kankare, M. Holopainen, X. Yu, J. Hyyppä, and H. Hyyppä, "Combination of individual tree detection and area-based approach in imputation of forest variables using airborne laser data," *ISPRS J. Photogramm. Remote Sens.*, vol. 67, pp. 73–79, 2012.

[24] P. Packalén and M. Maltamo, "The k-MSN method for the prediction of species-specific stand attributes using airborne laser scanning and aerial photographs," *Remote Sens. Environ.*, vol. 109, no. 3, pp. 328–341, 2007.

[25] A. T. Hudak *et al.*, "Regression modeling and mapping of coniferous forest basal area and tree density from discrete-return lidar and multispectral satellite data," *Can. J. Remote Sens.*, vol. 32, no. 2, pp. 126–138, 2006.

[26] J. W. Osborne and E. Waters, "Four assumptions of multiple regression that researchers should always test—Practical assessment, research & evaluation," *Pract. Assessment, Res. Eval.*, vol. 8, no. 2, pp. 1–5, 2002.

[27] V. Junttila, T. Kauranne, A. O. Finley, and J. B. Bradford, "Linear models for airborne-laser-scanning-based operational forest inventory with small field sample size and highly correlated LiDAR data," *IEEE Trans. Geosci. Remote Sens.*, vol. 53, no. 10, pp. 5600–5612, Oct. 2015.

[28] E. Næsset, "Estimation of above-and below-ground biomass in boreal forest ecosystems," *Int. Soc. Photogramm. Remote Sens. Int. Arch. Photogramm. Remote Sens. Spat. Inf. Sci.*, vol. 36, no. Jul., pp. 145–148, 2004.

[29] J. García-Gutiérrez, F. Martínez-Álvarez, A. Troncoso, and J. C. Riquelme, "A comparison of machine learning regression techniques for LiDAR-derived estimation of forest variables," *Neurocomputing*, vol. 167, pp. 24–31, 2015.

[30] G. Mountrakis, J. Im, and C. Ogole, "Support vector machines in remote sensing: A review," *ISPRS J. Photogramm. Remote Sens.*, vol. 66, no. 3, pp. 247–259, 2011.

[31] M. Belgiu and L. Dra, "Random forest in remote sensing: A review of applications and future directions," *ISPRS J. Photogramm. Remote Sens.*, vol. 114, pp. 24–31, 2016.

[32] A. K. Jain, J. Mao, and K. M. Mohiuddin, "Artificial neural networks: A tutorial," *Computer*, vol. 29, no. 3, pp. 31–44, Mar. 1996.

[33] R. Özçelik, M. J. Diamantopoulou, F. Crecente-Campo, and U. Eler, "Estimating Crimean juniper tree height using nonlinear regression and artificial neural network models," *Forest Ecol. Manage.*, vol. 306, pp. 52–60, 2013.

[34] M. H. Nunes and E. B. Görgens, "Artificial intelligence procedures for tree taper estimation within a complex vegetation mosaic in Brazil," *PLoS One*, vol. 11, May 2016, Art. no. e0154738.

[35] A. Carrio, C. Sampedro, A. Rodriguez-ramos, and P. Campoy, "A review of deep learning methods and applications for unmanned aerial vehicles," *J. Sens.*, vol. 2017, 2017, Art. no. 3296874.

[36] S. The, S. Ai, I. Dalle, and S. Galleria, "Deep learning in neural networks: An overview," pp. 1–88, 2014.

[37] Y. Lecun, Y. Bengio, and G. Hinton, "Deep learning," *Nature*, vol. 521, pp. 436–444, 2015.

[38] J. Schmidhuber, "Deep learning in neural networks: An overview," *Neural Networks*, vol. 61, pp. 85–117, 2015.

[39] M. Zhu, Y. He, and Q. He, "A review of researches on deep learning in remote sensing application," *Int. J. Geosci.*, vol. 2019, pp. 1–11, 2019.

[40] X. X. Zhu *et al.*, "Deep learning in remote sensing: A comprehensive review and list of resources," *IEEE Geosci. Remote Sens. Mag.*, vol. 5, no. 4, pp. 8–36, 2017.

[41] S. J. Russell and P. Norvig, *Artificial Intelligence: A Modern Approach*. London, U.K.: Pearson, 2016.
[42] W. Zhao and S. Du, "Learning multiscale and deep representations for classifying remotely sensed imagery," *ISPRS J. Photogramm. Remote Sens.*, vol. 113, pp. 155–165, 2016, doi: 10.1016/j.isprsjprs.2016.01.004.
[43] X. Chen, S. Xiang, C.-L. Liu, and C.-H. Pan, "Vehicle detection in satellite images by hybrid deep convolutional neural networks," *IEEE Geosci. Remote Sens. Lett.*, vol. 11, no. 10, pp. 1797–1801, Oct. 2014.
[44] M. Schmitt and X. X. Zhu, "Data fusion and remote sensing: An ever-growing relationship," *IEEE Geosci. Remote Sens. Mag.*, vol. 4, no. 4, pp. 6–23, Dec. 2016.
[45] J. Han, D. Zhang, G. Cheng, L. Guo, and J. Ren, "Object detection in optical remote sensing images based on weakly supervised learning and high-level feature learning," *IEEE Trans. Geosci. Remote Sens.*, vol. 53, no. 6, pp. 3325–3337, Jun. 2015.
[46] S. H. Khan, X. He, F. Porikli, and M. Bennamoun, "Forest change detection in incomplete satellite images with deep neural networks," *IEEE Trans. Geosci. Remote Sens.*, vol. 55, no. 9, pp. 5407–5423, Sep. 2017.
[47] L. Mou, P. Ghamisi, and X. X. Zhu, "Deep recurrent neural networks for hyperspectral image classification," *IEEE Trans. Geosci. Remote Sens.*, vol. 55, no. 7, pp. 3639–3655, Jul. 2017.
[48] C. P. Schwegmann, W. Kleynhans, B. P. Salmon, L. W. Mdakane, and R. G. V Meyer, "Very deep learning for ship discrimination in synthetic aperture radar imagery," in *Proc. IEEE Int. Geosci. Remote Sens. Symp.*, 2016, pp. 104–107.
[49] W. Liu, J. Sun, W. Li, T. Hu, and P. Wang, "Deep learning on point clouds and its application: A survey," *Sensors*, vol. 19, no. 19, 2019, Art. no. 4188.
[50] L. Zhong, L. Hu, and H. Zhou, "Deep learning based multi-temporal crop classification," *Remote Sens. Environ.*, vol. 221, pp. 430–443, 2019.
[51] W. Hu, Y. Huang, L. Wei, F. Zhang, and H. Li, "Deep convolutional neural networks for hyperspectral image classification," *J. Sensors*, vol. 2015, 2015, Art. no. 258619.
[52] K. Makantasis, K. Karantzalos, A. Doulamis, and N. Doulamis, "Deep supervised learning for hyperspectral data classification through convolutional neural networks," in *Proc. IEEE Int. Geosci. Remote Sens. Symp.*, 2015, pp. 4959–4962.
[53] L. Mou, P. Ghamisi, and X. X. Zhu, "Unsupervised spectral–spatial feature learning via deep residual Conv–Deconv network for hyperspectral image classification," *IEEE Trans. Geosci. Remote Sens.*, vol. 56, no. 1, pp. 391–406, Jan. 2017.
[54] L. Mou and X. X. Zhu, "RiFCN: Recurrent network in fully convolutional network for semantic segmentation of high resolution remote sensing images," 2018, *arXiv1805.02091*.
[55] H. Guan, Y. Yu, Z. Ji, J. Li, and Q. Zhang, "Deep learning-based tree classification using mobile LiDAR data," *Remote Sens. Lett.*, vol. 6, no. 11, pp. 864–873, 2015.
[56] J. Wang *et al.*, "Individual rubber tree segmentation based on ground-based LiDAR data and faster R-CNN of deep learning," *Forests*, vol. 10, no. 9, 2019, Art. no. 793.
[57] C. R. Qi, H. Su, K. Mo, and L. J. Guibas, "PointNet: Deep learning on point sets for 3D classification and segmentation," in *Proc. IEEE Conf. Comput. Vis. Pattern Recognit.*, 2017, pp. 652–660.
[58] C. R. Qi, L. Yi, H. Su, and L. J. Guibas, "PointNet++: Deep hierarchical feature learning on point sets in a metric space," in *Proc. Neural Inf. Process. Syst. Conf.*, 2017, pp. 5099–5108.
[59] İ. Ercanlı, "Innovative deep learning artificial intelligence applications for predicting relationships between individual tree height and diameter at breast height," *Forest Ecosyst.*, vol. 7, pp. 1–18, 2020.
[60] Z. Liu, C. Peng, T. Work, J.-N. Candau, A. DesRochers, and D. Kneeshaw, "Application of machine-learning methods in forest ecology: Recent progress and future challenges," *Environ. Rev.*, vol. 26, no. 4, pp. 339–350, 2018.
[61] H. Su, Y. Yu, Q. Du, and P. Du, "Ensemble learning for hyperspectral image classification using tangent collaborative representation," *IEEE Trans. Geosci. Remote Sens.*, vol. 58, no. 6, pp. 3778–3790, Jun. 2020.
[62] B. Liu, X. Yu, A. Yu, P. Zhang, G. Wan, and R. Wang, "Deep few-shot learning for hyperspectral image classification," *IEEE Trans. Geosci. Remote Sens.*, vol. 57, no. 4, pp. 2290–2304, Apr. 2019.
[63] M. Rostami, S. Kolouri, E. Eaton, and K. Kim, "Deep transfer learning for few-shot SAR image classification," *Remote Sens.*, vol. 11, no. 11, 2019, Art. no. 1374.
[64] Y.-X. Wang and M. Hebert, "Learning to learn: Model regression networks for easy small sample learning," in *Proc. Eur. Conf. Comput. Vis.*, 2016, pp. 616–634.
[65] W. Li, Q. Guo, M. K. Jakubowski, and M. Kelly, "A new method for segmenting individual trees from the lidar point cloud," *Photogramm. Eng. Remote Sens.*, vol. 78, no. 1, pp. 75–84, 2012.
[66] L. Mehtätalo, S. de-Miguel, and T. G. Gregoire, "Modeling height-diameter curves for prediction," *Can. J. Forest Res.*, vol. 45, no. 7, pp. 826–837, 2015.
[67] X. Zhao, Q. Guo, Y. Su, and B.-L. Xue, "Improved progressive TIN densification filtering algorithm for airborne LiDAR data in forested areas," *ISPRS J. Photogramm. Remote Sens.*, vol. 117, pp. 79–91, Jul. 2016.
[68] E. Næsset and K.-O. Bjerknes, "Estimating tree heights and number of stems in young forest stands using airborne laser scanner data," *Remote Sens. Environ.*, vol. 78, no. 3, pp. 328–340, 2001.
[69] A. Shaikh, A. Hannan, R. Manza, and R. Ramteke, "Generalized regression neural network and radial basis function for heart disease diagnosis," *Int. J. Comput. Appl.*, vol. 13, pp. 7–13, Nov. 2010.
[70] M. Bianchini, P. Frasconi, and M. Gori, "Learning without local minima in radial basis function networks," *IEEE Trans. Neural Netw.*, vol. 6, no. 3, pp. 749–756, May 1995.
[71] T. Poggio and F. Girosi, "Networks for approximation and learning," *Proc. IEEE*, vol. 78, no. 9, pp. 1481–1497, Sep. 1990.
[72] M. Bataineh and T. Marler, "Neural network for regression problems with reduced training sets," *Neural Netw.*, vol. 95, pp. 1–9, 2017.
[73] F. Chollet, "Keras: The python deep learning library," *ASCL.*, p. ascl-1806, 2018.
[74] M. Abadi *et al.*, "Tensorflow: A system for large-scale machine learning," in 12th (USENIX) symposium on operating systems design and implementation ({OSDI} 16), pp. 265–283, 2016.
[75] D. P. Kingma and J. Ba, "Adam: A method for stochastic optimization," 2014, *arXiv1412.6980*.
[76] S. Ruder, "An overview of multi-task learning in deep neural networks," 2017, *arXiv1706.05098*.
[77] F. Agostinelli, M. Hoffman, P. Sadowski, and P. Baldi, "Learning activation functions to improve deep neural networks," 2014, *arXiv1412.6830*.
[78] N. Srivastava, G. Hinton, A. Krizhevsky, I. Sutskever, and R. Salakhutdinov, "Dropout: A simple way to prevent neural networks from overfitting," *J. Mach. Learn. Res.*, vol. 15, no. 1, pp. 1929–1958, 2014.
[79] G. H. Golub and C. F. Van Loan, *Matrix Computations*, vol. 3. Baltimore, MD, USA: JHU Press, 2012.
[80] Y. Bengio, "Lecture notes in computer science," Jun. 2012, doi: 10.1007/978-3-642-35289-8_26.
[81] G. I. Diaz, A. Fokoue-Nkoutche, G. Nannicini, and H. Samulowitz, "An effective algorithm for hyperparameter optimization of neural networks," *IBM J. Res. Develop.*, vol. 61, no. 4/5, pp. 1–9, 2017.
[82] T. D. Gedeon, "Data mining of inputs: Analysing magnitude and functional measures," *Int. J. Neural Syst.*, vol. 8, no. 2, pp. 209–218, 1997.
[83] B. M. Greenwell, B. C. Boehmke, and A. J. Mccarthy, "A simple and effective model-based variable importance measure," 2018, *arXiv: 1805.04755*.

Hao Liu was born in Huai'an, Jiangsu Province, China, in 1994. He received the bachelor's degree in geographic information science, in 2017 from Nanjing Forestry University, Nanjing, China, where he is currently working toward the Ph.D. degree, majoring in silviculture.

His research interests include the application of remote sensing in forestry, such as forest structural attribute estimation and forest change detection, using LiDAR data and deep learning algorithms.

Xin Shen received the B.S. degree in remote sensing science and technology from Jiangsu Normal University, Xuzhou, China, in 2013, and the M.S. degree in forestry, in 2016 from Nanjing Forestry University, Nanjing, China, where he is currently working toward the Ph.D. degree in silviculture.

His research interests include forest resource management and monitoring, forest biophysical and biochemical parameters estimation, and precision cultivation using hyperspectral and LiDAR data.

Mr. Shen was the recipient of the National Scholarship for Doctoral Candidate, the National Competition Award for Scientific and Technological Works of Agricultural and Forestry Universities, and Excellent Graduates of Forestry in China.

Lin Cao received the B.S. degree in geographic information science from Nanjing Normal University, Nanjing, China, in 2006, the M.S. degree in forest resources management from Nanjing Forestry University, Nanjing, China, in 2008, and the Ph.D. degree from the University of British Columbia, Vancouver, BC, Canada, in 2016.

He is a Professor with the Faculty of Forestry, Nanjing Forestry University. His research interests include LiDAR applications in forest inventory and management, UAV and their point cloud processing, forest biomass estimation, forest change detection, tree species classification, subtropical forest ecology, ecological modeling, and wildlife habitat.

Ting Yun received the bachelor's degree in computer science, the master's degree in power engineering, and the Ph.D. degree in computer science from the Nanjing University of Science and Technology, Nanjing, China.

He is currently a Professor with the School of Computer Science, Nanjing Forestry University, Nanjing, China. He is also a Postdoctoral Fellow with the School of Informatics and Computing, Southeast University, Nanjing, China. His research interests include computer vision, computer graphics, and LiDAR survey for forest applications.

Zhengnan Zhang was born in Nanjing, Jiangsu Province, China, in 1992. He received the master's degree in forest management, in 2018 from Nanjing Forestry University, Nanjing, China, where he is currently working toward the doctoral degree, majoring in silviculture.

His research interests include forestry remote sensing using passive and active remote sensing technology.

Xiaoyao Fu was born in Taihe, Anhui Province, China, in 1996. He received the bachelor's degree in geographic information science, in 2018 from Nanjing Forestry University, Nanjing, China, where he is currently working toward the master's degree in forest management.

His current research interests include multiscale inversion and dynamic monitoring of forest structure parameters of plain plantation forests with fixed-wing UAV stereo photography to measure point clouds.

Xinxin Chen was born in Nantong, Jiangsu Province, China, in 1995. She is currently working toward the master's degree with the College of Information Science and Technology, Nanjing Forestry University, Nanjing, China.

Her research interests include LiDAR data analysis and computer graphics.

Fangzhou Liu was born in 1995. He is currently working toward the master's degree with the College of Information Science and Technology, Nanjing Forestry University, Nanjing, China.

His main research interests include pattern recognition, machine learning, data mining image-and LiDAR-based segmentation, and reconstruction.